Reorientation of the High Mobility Plane in Pentacene-Based Carbon Nanotube Enabled Vertical Field Effect Transistors

Mitchell A. McCarthy,[†] Bo Liu,[‡] Ramesh Jayaraman,[†] Stephen M. Gilbert,[‡] Do Young Kim,[†] Franky So,[†] and Andrew G. Rinzler[‡,*]

[†]Department of Materials Science and Engineering and [‡]Department of Physics, University of Florida, Gainesville, Florida 32611, United States

ABSTRACT The large current densities attained by carbon nanotube enabled vertical field effect transistors using crystalline organic channel materials are somewhat unexpected given the known large anisotropy in the mobility of crystalline organics and their conventional ordering on dielectric surfaces which tends to orient their high mobility axes parallel to the surface. This seeming contradiction is resolved by the finding that the nanotubes induce a molecular ordering that reorients the high mobility axes to favor current flow in a direction perpendicular to the substrate surface.

KEYWORDS: vertical field effect transistor · X-ray diffraction · carbon nanotube · low voltage

The crystallographic stacking of organic molecules often leads to anisotropy in the electronic properties of their films which can differ by orders of magnitude along distinct crystallographic directions.[1] The exceptional performance of pentacene in lateral channel thin-film transistors owes much to a fortuitous crystallographic orientation that places its high mobility $a-b$ stacking plane parallel to the gate dielectric surface, which is also the plane of current flow between the source and drain electrodes.[2] The mobility of pentacene in a direction perpendicular to this plane is known to be orders of magnitude lower.[3−5] Accordingly, it would seem that pentacene and analogous molecules with similar stacking would be poor candidates for vertical field effect transistors where the source−drain current must flow in a direction perpendicular to the dielectric surface.

Nevertheless, we recently demonstrated record high on-state current densities in a carbon nanotube enabled vertical field effect transistor (CN-VFET) employing dinaphtho-thieno-thiophene (DNTT) as the organic channel.[6] DNTT has a molecular shape, stacking, and crystallographic orientation on dielectrics that is quite similar to that of pentacene.[7,8] High current density, at low source−drain voltage, is anticipated for the CN-VFET architecture because the channel length between the vertically stacked source and drain electrodes is just the thickness of the thin-film organic layer between them (Figure 1); and indeed, the on-state currents scaled roughly as anticipated for a simple reduction in the channel length compared to the much longer channel lengths of conventional lateral channel DNTT-based FETs. Such simple scaling however ignores the anisotropy in the electronic properties expected from the crystallographic orientation of the DNTT molecules on dielectrics.

This result suggested that the single wall carbon nanotube (CNT) source electrode, despite possessing only a dilute coverage of the dielectric substrate, reoriented the crystallographic axes of DNTT to force the high mobility $a-b$ plane to lie near vertical. Since conjugated organic molecules are known to π stack on graphitic surfaces[9,10] and are suggested to do so on carbon nanotubes,[11] such reorientation of the initially deposited molecules, nucleating a near vertical reorientation of the $a-b$ plane, at least over the nanotubes, seems plausible. Here we demonstrate pentacene-based CN-VFETs that similarly exhibit very high on-state currents. By X-ray diffraction (XRD), atomic force microscopy (AFM), and mobility measurements we provide conclusive evidence that the nanotubes induce a reorientation of the pentacene $a-b$ plane to the near vertical direction. Such reorientation further explains the high current densities afforded by the CN-VFET and why, in the face of pentacene's known anisotropy, the simple channel length scaling agrees with the measured current output.

*Address correspondence to rinzler@phys.ufl.edu.

Received for review October 11, 2010 and accepted November 23, 2010.

Published online December 9, 2010. 10.1021/nn102721v

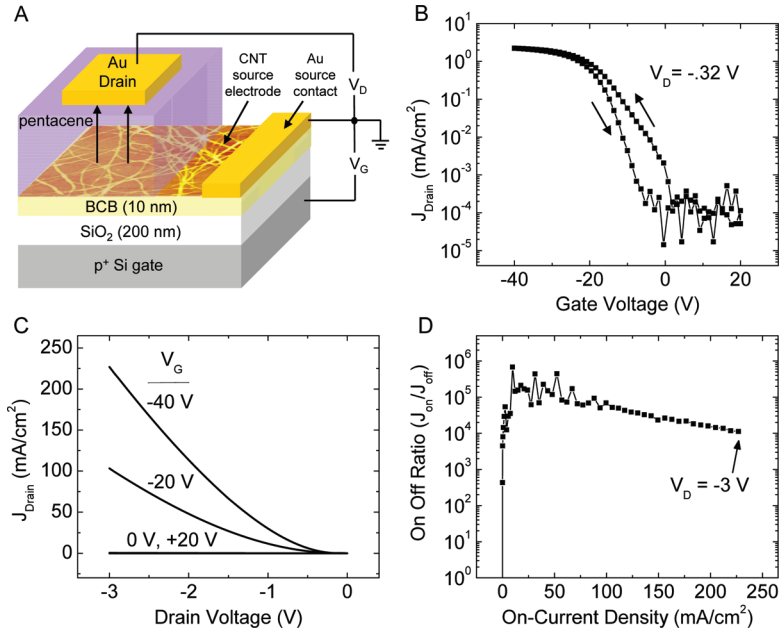

Figure 1. (A) Schematic of the CN-VFET with arrows depicting the direction holes flow in the on-state of the device. (B) Transfer curve of the CN-VFET with pentacene as the semiconductor layer shows a small amount of hysteresis over a gate voltage range of 60 V, with a subthreshold slope of 3.3 V/dec. (C) Output curves from V_G = 20 to −40 V in −20 V steps. (D) On/off ratio as a function of on-current density stays above 10^4 past 225 mA/cm^2 with a peak above 10^5 at ~20 mA/cm^2.

RESULTS AND DISCUSSION

Figure 1A shows the structure of the CN-VFET. The CN-VFET uses a bottom gate architecture and functions as a Schottky barrier transistor, where the height and width of the barrier for injecting holes from the CNT source into the pentacene layer are modulated by the gate electric field.[12] A thin (10 nm) hydrophobizing layer of cross-linked benzocyclobutene (BCB) deposited on the silicon oxide dielectric improves device performance.[13,14] Figure 1B shows the transfer characteristics for the device. With negative gate voltage, the hole injection barrier height and width are reduced allowing the drain current density (J_{Drain}) to reach 2.3 mA/cm^2 at a drain voltage (V_D, relative to the grounded nanotube source electrode) of only −0.32 V. Upon sweeping the gate voltage (V_G) toward 0 V, the device turns off. The relatively large gate voltage required to switch the current between the on- and off-state is due to the thick 200 nm SiO_2 gate dielectric used here. CN-VFETs exploiting a thin, high-k dielectric, switching comparable current densities for a gate voltage range of only ±2 V have recently been demonstrated.[6] The hysteresis seen in the transfer curve is due to charge traps and is virtually eliminated by limiting the gate voltage sweep range.[14] Figure 1C shows the output characteristics for the device. The drain current is ~225 mA/cm^2 at V_D = −3 V. On the basis of the area occupied by the devices, this current density approaches an order of magnitude larger current per unit device area than a recent state of the art TFT operating at a similar drain voltage.[6,8] Figure 1D plots the on/off ratio *versus* the on-state current density as V_D changes from 0 to −3 V. The on/off ratio hovers around 10^5 to J_{Drain} ~ 50 mA/cm^2 and remains above 10^4 to 225 mA/cm^2.

Figure 2A shows the herringbone molecular ordering for crystalline pentacene looking along the direction perpendicular to the (001) plane. Equivalent layers of molecules lie above and below the layer shown. The mobility along this direction is reported to be orders of magnitude lower than that along directions within the *a*−*b* plane (coplanar with (001)).[3−5] The mobility also varies within the *a*−*b* plane however the ratio between the in-plane highest and lowest mobilities is only 3.5.[15] When grown on dielectric surfaces the molecules tend to assume the nearly upright orientation that places the high mobility (001) planes parallel to the surface (Figure 2B shows the *b*-axis projection). This crystalline orientation is in contrast to pentacene deposited onto smooth gold and highly ordered pyrolytic graphite where the initially deposited molecules tend to lie flat, with subsequent layers assuming the herringbone stacking that orients the high mobility *a*−*b* plane to lie nearly perpendicular to the surface.[10,16,17]

To probe the crystalline orientation of pentacene grown on dilute nanotube networks on BCB (at a surface density relevant to CN-VFETs), we acquired θ−2θ X-ray diffraction data and AFM images for 560 nm of pentacene grown on three types of samples: (1) bare 10 nm thick BCB on glass; (2) dilute nanotube networks on BCB (10 nm) on glass and; (3) 45 nm thick nanotube films on glass, in which case the thick nanotube film provides no line of sight access for the evaporated pentacene to the underlying glass. The pentacene was deposited on the samples during the same growth run

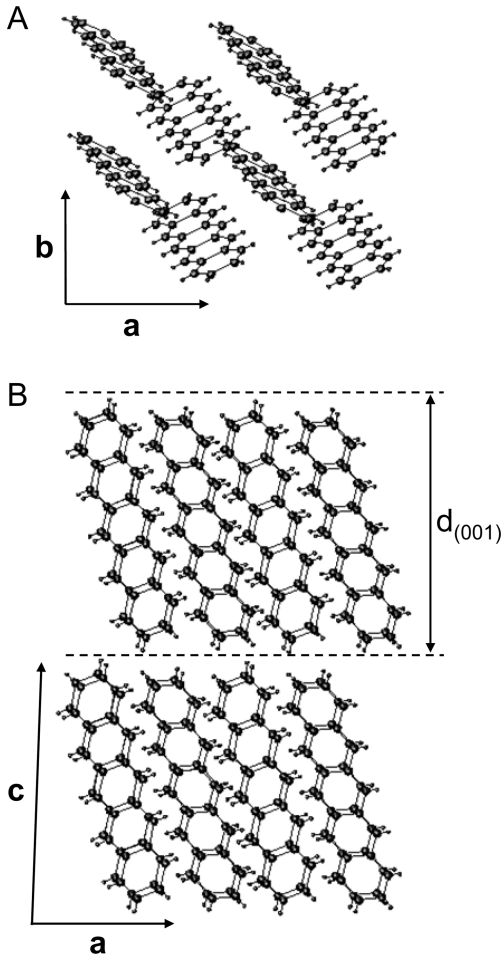

Figure 2. The crystal structure of pentacene. The *a*−*b* plane orients itself parallel to the oxide surface. (A) The herringbone packing arrangement of pentacene viewed from the direction perpendicular to the *a*−*b* plane. (B) The *b*-axis projection showing the slight tilt of the molecules as well as the (001) interplanar spacing ($d_{(001)}$).

under similar conditions used in fabrication of the CN-VFET (growth rate 1 Å/s, pressure $\sim 3 \times 10^{-7}$ Torr, room temperature substrate).

Figure 3 shows the θ−2θ X-ray diffraction plots for these samples. The pentacene on bare BCB XRD curve (bottom) shows clear pairs of (001), (002), (003), and (004) plane reflections. In each pair, the left peak is from the thin-film pentacene phase and the right peak is from the bulk phase.[18,19] These are consistent with the *a*−*b* plane parallel to the BCB surface. The (001) *d*-spacing extracted from these data yield values of 15.2 Å and 14.2 Å for the thin-film and bulk phases, respectively, in close agreement with the literature.[10,16,17,20] The pentacene on the 45 nm thick CNT film in contrast shows none of these reflections but rather only peaks at 19.3°, 24.1° and 28.3° corresponding to (110), (022) and (−201) plane reflections consistent with the *a*−*b* plane lying nearly perpendicular to the surface.[16] The θ−2θ plot of the pentacene on the dilute CNT network shares reflections from both of these cases indicating a mixed orientation of the crystallites. Taken together these results confirm the idea that the nanotubes nucleate a reorientation of the pentacene *a*−*b* plane to lie near perpendicular to the substrate surface in the vicinity of the nanotubes.

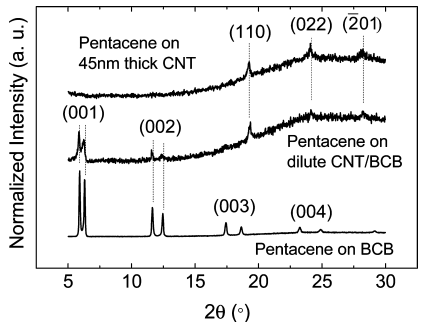

Figure 3. X-ray diffraction data taken in θ−2θ mode of pentacene grown on BCB (bottom), pentacene grown on dilute CNT on BCB (middle) and pentacene grown on 45 nm thick CNT film on glass (top).

Such reorientation of pentacene's crystalline axes on the nanotubes has dramatic effects on the pentacene layer morphology. Figure 4A shows the AFM image of the dilute nanotubes on BCB/glass at the surface density used in the CN-VFET and in these studies. Figures 4B-D show AFM images of pentacene grown on the samples discussed above: 4B - pentacene on bare BCB/glass; 4C - pentacene on the dilute CNT/BCB/glass and; 4D - pentacene on the 45 nm thick CNT film on glass. Also shown is the root-mean-square (rms) surface roughness measured for each sample. Dramatic difference between the crystallite morphology of pentacene on the bare BCB and the two nanotube samples is evident from these images and mirrored in the surface roughness. While the X-ray data evidenced regions of (001) plane crystallites in the dilute nanotube film sample, these crystalline grains are evidently kept much smaller by their confinement between the nanotube nucleated grains (Figure 4C) than appear on the bare BCB sample (Figure 4B).

Figure 5 illustrates a plausible molecular packing of pentacene, to scale, on the CNTs and the nearby BCB surface consistent with its ordering on graphite[10] and our XRD data. How precisely the pentacene molecules order in going around the nanotube bundle shown goes beyond the scope of this investigation. The average bundle diameter in our material is ~5 nm,[12] which correlates with the 7 hexagonal close packed nanotubes having individual diameters of ~1.4 nm,[21] drawn with a 1.7 nm center-to-center distance.[22]

From this confirmation that the nanotubes reorient the *a*−*b* plane to lie near perpendicular to the substrate we can only infer that pentacene has high mobility in a direction perpendicular to the substrate (the direction of current flow) in the CN-VFET. Therefore, a direct measure of the pentacene mobility in this direction, with and without the nanotubes is desirable. A method to estimate the mobility of a thin-film organic layer in the direction perpendicular to the layer is by

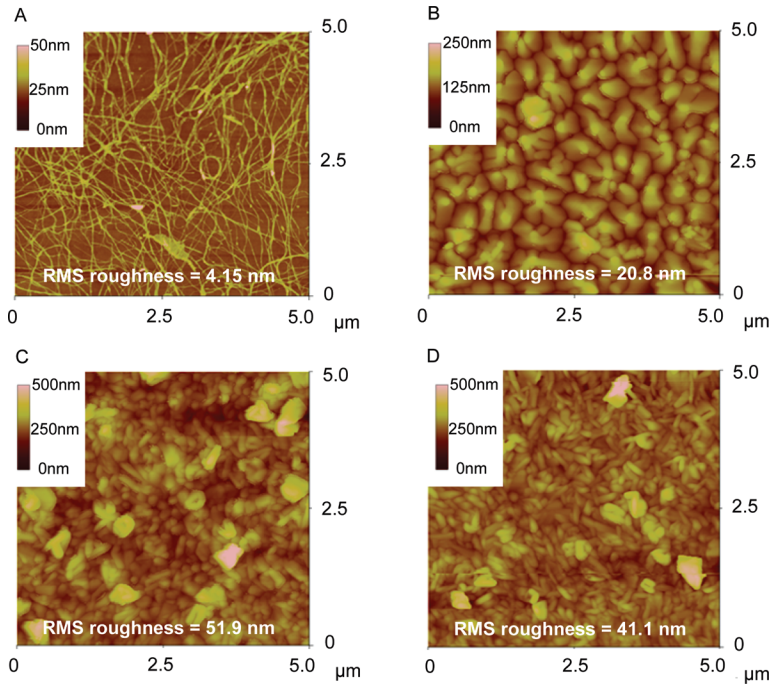

Figure 4. AFM micrographs of (A) a dilute CNT network on BCB/glass, (B) pentacene on BCB/glass, (C) pentacene on a dilute CNT network on BCB/glass and (D) pentacene on 45 nm thick CNT film on glass. Pentacene was thermally evaporated to a thickness of 560 nm at 1 Å/s with the substrate at room temperature at a pressure ~3 × 10^{-7} Torr

measuring and fitting $J-V$ curves at high fields in a sandwich-type, single carrier, metal−semiconductor−metal (MSM) device to the Mott−Gurney equation. This equation assumes ohmic injection and that the current−density has saturated to the space charge limited (SCL) regime, where $J \propto V^2$. The CN-VFET forms such a sandwich-type device. At the extreme gate voltage, where the injection barrier is minimized and the injection is most nearly ohmic, we looked for a V^2 dependence for J_{Drain}. However, as seen in the output curve of Figure 1C where $V_G = -40$ V, at the higher drain voltages, J_{Drain} saturates to a linear dependence on V_D. Calculating the series resistance that the slope there implies gives ~24 kΩ, which is close to the series resistance of the CNT electrode in the region between the CN-VFET element under test and its remote (~2 mm distant) Au source contact. This series resistance precludes extraction of the mobility by use of the Mott−Gurney equation directly from CN-VFET devices.

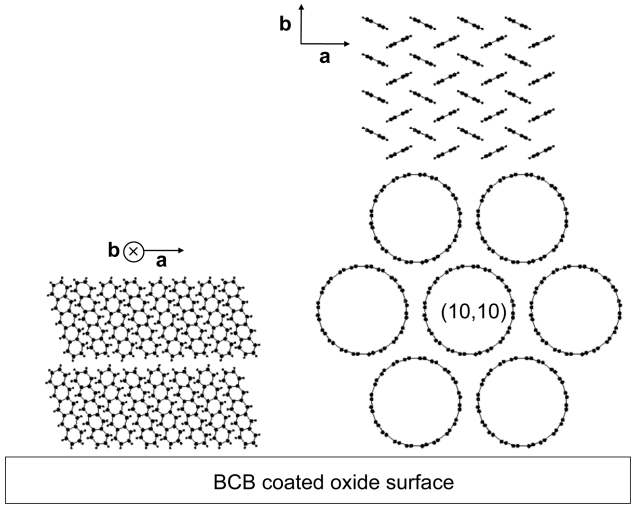

Figure 5. Scale model depicting the mixed orientation crystallites on the CNT bundle and partially covered BCB surface. Left - $a-b$ plane parallel to the surface for pentacene grains nucleated on BCB. Right - the $a-b$ plane along the near vertical direction for pentacene grains nucleated on a bundle of (10,10) nanotubes.

The series resistance of a remote contact to the nanotubes can be avoided if the dilute nanotube film were deposited directly onto a conductor and if this composite electrode formed one side of the M*SM (M* = composite electrode, S = pentacene, and M = Au) structure for the $J-V$ measurement. For such a measurement to have relevance to the mobility of the pentacene in the crystalline orientation that it assumes in the CN-VFET, however, two issues must be addressed. First, the pentacene must orient on the bare conductor in the same orientation it assumes on oxide, and other, dielectrics (*i.e.*, with its $a-b$ plane parallel to the surface). Gold, which does not generally yield such an orientation, is precluded, but indium tin oxide (ITO), being both conductive and an oxide, came to mind as a potentially suitable candidate electrode. Below we provide XRD data showing that pentacene on bare UV ozone treated ITO indeed assumes the needed crystalline orientation ($a-b$ plane parallel to the surface). Thus ITO can act as the surrogate for the dielectric layer (in the sense of the pentacene crystalline orientation) in an M*SM device permitting comparison between the mobility in a direction perpendicular to the pentacene layer, both with

and without the nanotubes present. The second issue that must be addressed in such an experiment is the Schottky barrier that develops between the pentacene and the electrode. In the MSM configuration there is no gate field available to reduce this barrier, but application of the Mott−Gurney expression requires near ohmic injection (the barrier must be small enough to allow the current to be space charge limited rather than contact limited at the voltages used to fit the V^2 dependence). It has been shown that barriers for injecting holes into organic semiconductors can be minimized by a dilute doping with tetrafluorotetracyanoquinodimethane (F4-TCNQ) in a thin interfacial layer between the electrode and the rest of the undoped organic layer.[23] Since such doping may also modify the crystalline orientation of the pentacene on the ITO, it must be confirmed that it does not do so. This then formed our strategy for the experiments performed and the data that follows:

(1) Confirm by XRD that pentacene deposited on ITO with the first 8 nm doped by F4-TCNQ results in a crystalline orientation that places the pentacene $a-b$ plane parallel to the surface.
(2) Confirm by XRD that a dilute nanotube layer on the ITO induces the crystalline reorientation of the pentacene (with 8 nm F4-TCNQ doped interfacial layer) over the nanotubes generating the mixed grain orientations.
(3) Compare the surface morphology of these samples by AFM.
(4) Construct M*SM samples where M* = bare ITO or ITO with a dilute nanotube layer, S = pentacene in which the first 8 nm are 1% F4-TCNQ doped, and M = Au.
(5) Measure the $J-V$ curves for these samples and look at high fields for a V^2 dependence to fit the mobilities using the Mott−Gurney equation.

Figure 6A shows the XRD data for the pentacene/ITO and pentacene/nanotube/ITO samples. Figure 6B and C shows AFM images of these respective samples providing their surface morphology and root-mean square (rms) roughness. From the XRD data of the pentacene on bare ITO, we find only peaks consistent with the $a-b$ plane lying parallel to the surface. The pentacene on nanotube/ITO sample in contrast shows the expected mixed phase. The pentacene crystalline grains on ITO (Figure 6B) are much smaller than they are on BCB (Figure 4B), though the surface roughness is comparable. This could be due to the microcrystalline nature of the underlying ITO (note the ITO (211) reflection[24] in the XRD data) compared to the amorphous nature of the much smoother underlying BCB (BCB rms roughness was <0.5 nm compared to 4.5 nm for the ITO, as measured by AFM, images not shown). The morphology of the pentacene on the nanotube/ITO sample (Figure 6C) and its rms surface roughness, however,

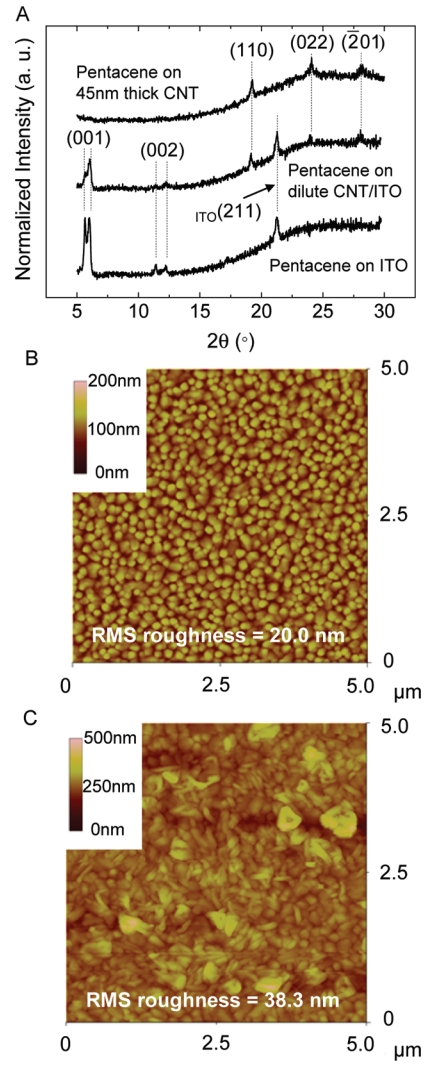

Figure 6. (A) XRD data taken in θ−2θ mode of pentacene grown on ITO (bottom), on dilute CNT on ITO (middle), and on a 45 nm thick CNT film on glass (top). AFM micrographs of: (B) pentacene on ITO and (C) pentacene on a dilute CNT network on ITO. Pentacene was thermally evaporated to a thickness of 560 nm at 1 Å/s on a room temperature substrate at a pressure ~3 × 10^{-7} Torr.

are quite similar to those of pentacene on the nanotube/BCB sample (Figure 4C).

Figure 7A and B illustrates the two types of M*SM (M* = bare ITO or nanotubes on ITO) devices studied, and Figure 7C compares the $J-V$ (log−log) plots for the two types of devices. Also shown in Figure 7C is a line for which $J \propto V^2$. At the larger applied voltages the data clearly follow a V^2 dependence, indicating the applicability of the Mott−Gurney expression. In the trap-free limit for SCL current density this equation is

$$J_{SCL} = \frac{9}{8}\varepsilon_r\varepsilon_0\mu_{SCL}\frac{V^2}{L^3} \quad (1)$$

where ε_r is the relative permittivity, μ_{SCL} the SCL mobility, V the applied voltage, and L the thickness of the semiconductor layer.

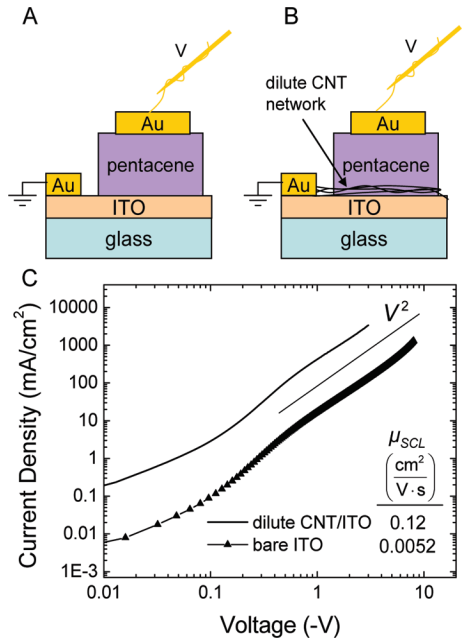

Figure 7. Schematics of the pentacene M*SM hole-only devices fabricated for measurement of μ_{SCL}. (A) Pentacene on ITO device and (B) pentacene on dilute CNT/ITO device. (C) $J-V$ curves of the three devices. The mobility values in the lower right corner of (C) are extracted from fitting eq 1 to the $J-V$ curves shown. Both devices follow a V^2 dependence, as indicated by the V^2 reference line in (C).

To determine μ_{SCL} the relative permittivity of pentacene must be determined. Values cited in the literature range from 3.7 to 6.[25−27] To obtain a more precise value (relevant to pentacene grown under our conditions), we fabricated parallel plate capacitors using aluminum electrodes and pentacene as the sandwiched dielectric. Al was chosen because its workfunction relative to the transport levels of pentacene renders it a noninjecting electrode. From the device dimensions and the measured capacitance (further details given in the Supporting Information), the relative permittivity was determined to be 5.4 ± 0.3.

With this information, eq 1 can be used to fit the $J-V$ plots in Figure 7C to yield mobilities, in a direction perpendicular to the substrate, of 0.0052 $cm^2/(V \cdot s)$ for the pentacene on ITO (pentacene $a-b$ plane parallel to substrate) and 0.12 $cm^2/(V \cdot s)$ for the pentacene on nanotubes/ITO (pentacene $a-b$ planes both parallel and perpendicular to the substrate). Thus, for a pentacene film on a substrate that normally takes on a crystalline orientation having its $a-b$ plane parallel to the substrate, the mobility in a direction perpendicular to the substrate is 23 times greater in the presence of nanotubes (at the density used in the CN-VFET) than without the nanotubes, and this difference is directly attributable to the reorientation of the pentacene crystalline orientation induced by the nanotubes. In arriving at this mobility anisotropy factor, we neglected to account, however, for the anisotropy in the permittivity. Recent theory has indicated a permittivity of 5.3 for the direction along the long molecular axis (very close to the value from our capacitance measurement on aluminum) but approximately half of this value in directions perpendicular to the long molecular axis.[28] Since the orientation of pentacene on the nanotubes would conform to the latter case, the mobility anisotropy would increase to approximately $2 \times 23 = 46$. This still falls well short of the factors of 450 and 160 attributed to the mobility anisotropy of single-crystal pentacene along the *b- versus c*-axis and *a- versus c*-axis, respectively,[4] but this is readily explained by the orientationally mixed phase on the dilute nanotube network samples.

CONCLUSIONS

Based on these results, in addition to its short channel length, the very high on-state currents seen in the pentacene-based CN-VFET can be (partially) attributed to a reorientation of the pentacene crystalline axes to a direction that is advantageous to the device architecture. Since as a general rule for planar crystalline organic molecules, the high-mobility direction lies along the direction in which the molecules π or herringbone stack, such advantageous reorientation should occur for most planar organics used as the channel material in the CN-VFET.

METHODS

CN-VFET Fabrication. CN-VFETs were fabricated on heavily p-doped Si substrates with a thermally grown 200 nm thick SiO_2 dielectric. The low-k spin-on polymer BCB (trade name cyclotene, Dow Chemical Co.) was diluted in trimethylbenzene (Dow Chemical Co. rinse solvent RS T1100) and spin coated at 3000 rpm for 45 s inside an Ar glovebox. It was soft baked at 100 °C for 20 min and hard baked at 250 °C for 1 h. During the hard bake, BCB cross-links and becomes insoluble to the subsequent solvents used in the transfer of the single wall carbon nanotube (CNT) source electrode. The thickness of BCB film was ~10 nm. All deposited film thicknesses were determined by AFM step height measurements at razor blade generated scratches in the corresponding films down to the hard glass or SiO2 surface. A Cr/Au (10/50 nm, respectively) source contact electrode was deposited on the BCB film in vacuum at $\sim 8 \times 10^{-7}$ Torr, at 2.0 Å/s. Using the Cr/Au source contacts for alignment, a prefabricated dilute CNT network was transferred (as described previously)[29] in ambient atmosphere onto the BCB film overlapping the Cr/Au contact. Following transfer of the CNT network, the device was baked at 225 °C for 1 h on a hot plate in an Ar glovebox. From this point forward through electrical characterization, the device stayed in the Ar glovebox without exposure to the ambient. In an evaporator integrated into the glovebox pentacene (Aldrich, sublimed grade 99.9% purity) was deposited onto the CNT film, through a shadow mask, at a pressure of $\sim 3 \times 10^{-7}$ Torr and a rate of 2.75 Å/s to a thickness of 350 nm (substrate at room temperature). The sample was subsequently transferred to a second metals evaporator within the same glovebox for deposition of the Au drain electrode. An indium dot was used to form the gate contact pressing the dot into a line scratched through the SiO_2/BCB dielectric layers with a diamond tip scribe.

CN-VFET devices were electrically measured with a home-built probe station inside the same Ar glovebox in which they were fabricated. Transistor output and transfer curves were recorded with a two channel Keithley 2612A system sourcemeter controlled by a program written in LabVIEW.

X-ray Diffraction Samples and M*SM-Type Hole-Only Devices. For the non-ITO containing samples, glass microscope slides were diced and cleaned before depositions. For the BCB coated samples, BCB was deposited and cured the same way as in the CN-VFET. For the ITO samples, 5−15 Ω/□ ITO on glass from Delta Technologies was cleaned and diced before deposition of the subsequent layers. Cr/Au contact electrodes (10/50 nm, respectively) were deposited, by the same method as the CN-VFET, onto the ITO of the two M*SM-type devices. An ultraviolet (UV) ozone treatment for 20 min was carried out on the bare ITO samples. For the dilute CNT network on BCB/glass sample and the dilute CNT network on ITO, a dilute CNT network with the same density of CNTs/area as in the CN-VFET was transferred to the sample, as above. For the thick CNT film on glass sample, a 45 nm CNT film was transferred, as above. The dilute CNT network was deposited overlapping the Cr/Au ITO contacts and extending over the bare ITO in the area beneath where the pentacene and Au layers were subsequently evaporated. On the two sandwich-type devices and one bare ITO XRD sample, 8 nm of pentacene doped with 1 vol % tetrafluorotetracyanoquinodimethane (F4-TCNQ) was deposited immediately following the UV ozone treatment of the bare ITO M*SM and XRD samples. The doped layer was deposited by codeposition at a chamber pressure of $\sim 3 \times 10^{-7}$ Torr, on a room temperature substrate with a pentacene growth rate of 1 Å/s and an F4-TCNQ growth rate of 0.01 Å/s. After the doped layer was deposited, the five XRD samples were loaded into the deposition chamber, and the neat pentacene layer was deposited on all eight samples simultaneously to a thickness of 560 nm at a chamber pressure of $\sim 3 \times 10^{-7}$ Torr (substrates at room temperature). For the samples to be used for the mobility measurements, 50 nm of Au was patterned through a shadow mask yielding a top contact with the same size and shape as the CN-VFET drain contact.

XRD samples were measured with a Philips APD 3720 operated in $\theta-2\theta$ mode (Cu $K_{\alpha 1}$, $\lambda = 1.541$ Å). Continuous scans from $2\theta = 5°$ to 30° in increments of 0.02° with a 4 s integration time were taken on all samples.

In addition to the XRD data shown, XRD scans were also recorded for:

(1) A 45 nm CNT film on glass without pentacene, which showed no peaks.
(2) A bare ITO/glass sample without pentacene which showed the (211) peak associated with ITO.
(3) The 8 nm doped /560 nm neat pentacene samples which showed the same peaks as the neat pentacene only XRD sample thereby confirming that F4TCNQ doping does not modify the orientation of the subsequently deposited neat pentacene layer.

Sandwich-type hole-only devices were exposed to the ambient environment for 30 min before electrical measurements. *J*−*V* data was recorded with a Keithley 2612A system sourcemeter controlled by a program written in LabVIEW.

Metal−Insulator−Metal Capacitors. Glass microscope slides were diced, cleaned, and served as the substrates for the metal−insulator−metal capacitors. The bottom and top electrodes were 60 nm of thermally evaporated Al patterned through a shadow mask. After deposition of the bottom electrode, without exposing to the ambient, pentacene was grown to 165 nm on one substrate and 330 nm on another. Pentacene was deposited at 2.6 Å/s at a pressure of $\sim 3 \times 10^{-7}$ Torr. Circular-shaped top electrodes were defined in two diameters, 0.86 and 1.3 mm. Capacitance was measured with an HP 4284A Precision LCR meter at 1 kHz at a voltage amplitude of 100 mV, operated in parallel capacitance−resistance (C_p-R_p) mode.

Acknowledgment. We are grateful for support from the National Science Foundation under ECCS-0824157 and from Nanoholdings, LLC. We also acknowledge the use of XRD equipment and technical support from the University of Florida Major Analytical Instrumentation Center (MAIC). We thank Prof. Art Hebard and Dr. Sefaattin Tongay for use of and assistance with the HP capacitance LCR meter.

Supporting Information Available: Additional data of the capacitance measurements for extraction of the relative permittivity of pentacene. This material is available free of charge *via* the Internet at http://pubs.acs.org.

REFERENCES AND NOTES

1. Sirringhaus, H.; Brown, P. J.; Friend, R. H.; Nielsen, M. M.; Bechgaard, K.; Langeveld-Voss, B. M. W.; Spiering, A. J. H.; Janssen, R. A. J.; Meijer, E. W.; Herwig, P. D. M.; et al. Two-Dimensional Charge Transport in Self-Organized, High-Mobility Conjugated Polymers. *Nature* **1999**, *401*, 685–688.
2. Dimitrakopoulos, C. D.; Brown, A. R.; Pomp, A. Molecular Beam Deposited Thin Films of Pentacene for Organic Field Effect Transistor Applications. *J. Appl. Phys.* **1996**, *80*, 2501–2508.
3. Hu, W. S.; Tao, Y. T.; Chen, Y. F.; Chang, C. S. Orientation-Dependent Conductance Study of Pentacene Nanocrystals by Conductive Atomic Force Microscopy. *Appl. Phys. Lett.* **2008**, *93*, 3304.
4. Jurchescu, O. D.; Baas, J.; Palstra, T. T. M. Effect of Impurities on the Mobility of Single Crystal Pentacene. *Appl. Phys. Lett.* **2004**, *84*, 3061–3063.
5. Ohashi, N.; Tomii, H.; Sakai, M.; Kudo, K.; Nakamura, M. Anisotropy of Electrical Conductivity in a Pentacene Crystal Grain on SiO_2 Evaluated by Atomic-Force-Microscope Potentiometry and Electrostatic Simulation. *Appl. Phys. Lett.* **2010**, *96*, 3302.
6. McCarthy, M. A.; Liu, B.; Rinzler, A. G. High Current, Low Voltage Carbon Nanotube Enabled Vertical Organic Field Effect Transistors. *Nano Lett.* **2010**, *10*, 3467.
7. Yamamoto, T.; Takimiya, K. Facile Synthesis of Highly Pi-Extended Heteroarenes, Dinaphtho[2,3-b: 2′,3′-f]chalcogenopheno[3,2-b]chalcogenophenes, and Their Application to Field-Effect Transistors. *J. Am. Chem. Soc.* **2007**, *129*, 2224–2225.
8. Zschieschang, U.; Ante, F.; Yamamoto, T.; Takimiya, K.; Kuwabara, H.; Ikeda, M.; Sekitani, T.; Someya, T.; Kern, K.; Klauk, H. Flexible Low-Voltage Organic Transistors and Circuits Based on a High-Mobility Organic Semiconductor with Good Air Stability. *Adv. Mater.* **2010**, *22*, 982.
9. Harada, Y.; Ozaki, H.; Ohno, K. Selective Observation of Outermost Surface-Layer during Epitaxial-Growth by Penning-Ionization Electron-Spectroscopy - Pentacene on Graphite. *Phys. Rev. Lett.* **1984**, *52*, 2269–2272.
10. Gotzen, J.; Kafer, D.; Woll, C.; Witte, G. Growth and Structure of Pentacene Films on Graphite: Weak Adhesion as a Key for Epitaxial Film Growth. *Phys. Rev. B: Condens. Matter Mater. Phys.* **2010**, *81*, 5440.
11. Cao, Q.; Zhu, Z. T.; Lemaitre, M. G.; Xia, M. G.; Shim, M.; Rogers, J. A. Transparent Flexible Organic Thin-Film Transistors That Use Printed Single-Walled Carbon Nanotube Electrodes. *Appl. Phys. Lett.* **2006**, *88*, 3511.
12. Liu, B.; McCarthy, M. A.; Yoon, Y.; Kim, D. Y.; Wu, Z. C.; So, F.; Holloway, P. H.; Reynolds, J. R.; Guo, J.; Rinzler, A. G. Carbon-Nanotube-Enabled Vertical Field Effect and Light-Emitting Transistors. *Adv. Mater.* **2008**, *20*, 3605.
13. Chua, L. L.; Zaumseil, J.; Chang, J. F.; Ou, E. C. W.; Ho, P. K. H.; Sirringhaus, H.; Friend, R. H. General Observation of n-type Field-Effect Behavior in Organic Semiconductors. *Nature* **2005**, *434*, 194–199.
14. Liu, B.; McCarthy, M. A.; Rinzler, A. G. Non-Volatile Organic Memory Elements Based on Carbon Nanotube Enabled Vertical Field Effect Transistors. *Adv. Funct. Mat.* **2010**, *20*, 3440.
15. Lee, J. Y.; Roth, S.; Park, Y. W. Anisotropic Field Effect Mobility in Single Crystal Pentacene. *Appl. Phys. Lett.* **2006**, *88*, 2106.
16. Hu, W. S.; Tao, Y. T.; Hsu, Y. J.; Wei, D. H.; Wu, Y. S. Molecular Orientation of Evaporated Pentacene Films on Gold: Alignment Effect of Self-Assembled Monolayer. *Langmuir* **2005**, *21*, 2260–2266.

17. Kafer, D.; Ruppel, L.; Witte, G. Growth of Pentacene on Clean and Modified Gold Surfaces. *Phys. Rev. B: Condens. Matter Mater. Phys.* **2007**, *75*, 5309.
18. Campbell, R. B.; Trotter, J.; Monteath, J. Crystal Structure of Hexacene, and a Revision of Crystallographic Data for Tetracene and Pentacene. *Acta Crystallogr.* **1962**, *15*, 289.
19. Yoshida, H.; Inaba, K.; Sato, N. X-ray Diffraction Reciprocal Space Mapping Study of the Thin Film Phase of Pentacene. *Appl. Phys. Lett.* **2007**, *90*, 1930.
20. Knipp, D.; Street, R. A.; Volkel, A.; Ho, J. Pentacene Thin Film Transistors on Inorganic Dielectrics: Morphology, Structural Properties, and Electronic Transport. *J. Appl. Phys.* **2003**, *93*, 347–355.
21. Rinzler, A. G.; Liu, J.; Dai, H.; Nikolaev, P.; Huffman, C. B.; Rodriguez-Macias, F. J.; Boul, P. J.; Lu, A. H.; Heymann, D.; Colbert, D. T.; Lee, R. S.; Fischer, J. E.; Rao, A. M.; Eklund, P. C.; Smalley, R. E. Large-Scale Purification of Single-Wall Carbon Nanotubes: Process, Product, and Characterization. *Appl. Phys. A: Mater. Sci. Process.* **1998**, *67*, 29–37.
22. Thess, A.; Lee, R.; Nikolaev, P.; Dai, H. J.; Petit, P.; Robert, J.; Xu, C. H.; Lee, Y. H.; Kim, S. G.; Rinzler, A. G.; et al. Crystalline Ropes of Metallic Carbon Nanotubes. *Science* **1996**, *273*, 483–487.
23. Gao, W. Y.; Kahn, A. Controlled p Doping of the Hole-Transport Molecular Material N, N ′-diphenyl-N, N ′-bis(1-naphthyl)-1,1(′)-biphenyl-4,4 ′-diamine with tetrafluorotetracyanoquinodimethane. *J. Appl. Phys.* **2003**, *94*, 359–366.
24. Thilakan, P.; Minarini, C.; Loreti, S.; Terzini, E. Investigations on the Crystallization Properties of RF Magnetron Sputtered Indium Tin Oxide Thin Films. *Thin Solid Films* **2001**, *388*, 34–40.
25. Lee, J.; Kim, S. S.; Kim, K.; Kim, J. H.; Im, S. Correlation Between Photoelectric and Optical Absorption Spectra of Thermally Evaporated Pentacene Films. *Appl. Phys. Lett.* **2004**, *84*, 1701–1703.
26. Mun, S. J.; Choi, J. M.; Lee, K. H.; Lee, K.; Im, S. Determining the Optimum Pentacene Channel Thickness on Hydrophobic and Hydrophilic Dielectric Surface. *Appl. Phys. Lett.* **2008**, *93*, 3301.
27. Shimada, T.; Saiki, K. Electron Energy Loss Spectroscopy of Ultrathin Pentacene Field Effect Transistors. *J. Electron Spectrosc. Relat. Phenom.* **2007**, *154*, 119–122.
28. Tsiper, E. V.; Soos, Z. G. Electronic Polarization in Pentacene Crystals and Thin Films. *Phys. Rev. B: Condens. Matter Mater. Phys.* **2003**, *68*, 5301.
29. Wu, Z. C.; Chen, Z. H.; Du, X.; Logan, J. M.; Sippel, J.; Nikolou, M.; Kamaras, K.; Reynolds, J. R.; Tanner, D. B.; Hebard, A. F.; et al. Transparent, Conductive Carbon Nanotube Films. *Science* **2004**, *305*, 1273–1276.